Article

Effect of new analogs of hexyloxy phenyl imidazoline on *quorum sensing* in *Chromobacterium violaceum* and *in silico* analysis of ligand-receptor interactions

José Luis Herrera-Arizmendi,[1] Everardo Curiel-Quesada,[2] José Correa-Basurto,[3] Martiniano Bello[3] and Alicia Reyes-Arellano[1,*]

[1] Instituto Politécnico Nacional, Escuela Nacional de Ciencias Biológicas, Departamento de Química Orgánica. Carpio y Plan de Ayala S/N. Colonia Santo Tomás. 11340 Ciudad de México. México. E-mail: areyesarellano@yahoo.com.mx

[2] Instituto Politécnico Nacional, Escuela Nacional de Ciencias Biológicas, Departamento de Bioquímica. Carpio y Plan de Ayala S/N. Colonia Santo Tomás. 11340 Ciudad de México, México. E-mail: ecqmixcoacdf@gmail.com

[3] Instituto Politécnico Nacional, Escuela Superior de Medicina, Laboratorio de Diseño y Desarrollo de Nuevos Fármacos e Innovación Biotecnológica. 11340 Ciudad de México. México. E-mail: bellomartini@gmail.com; corrjose@gmail.com

* Correspondence: E-mail: areyesarellano@yahoo.com.mx. Tel.: +52-55-57296000 extension 62526.

Received: date; Accepted: date; Published: date

Abstract: The increasingly common occurrence of antibiotic-resistant bacteria has become an urgent public health issue. There are currently some infections without any effective treatment, which require new therapeutic strategies. An attractive alternative is the design of compounds capable of disrupting bacterial communication known as *quorum sensing* (QS). In gram-negative bacteria, such communication is regulated by acyl-homoserine lactones (AHLs). QS allows bacteria to proliferate before expressing virulence factors. Our group previously reported that hexyloxy phenyl imidazoline (**9**) demonstrated 71% inhibitory activity of QS at 100 μM (IC50=90.9 μM) in *Chomobacterium violaceum,* a gram-negative bacterium. The aim of the present study was to take **9** as a lead compound to design and synthesize three 2-imidazolines (**13**-**15**) and three 2-oxazolines (**16**-**18**), to be evaluated as *quorum sensing* inhibitors on *C. violaceum* CV026. We were looking for compounds with a higher affinity towards the Cvi receptor of this bacterium and the ability to inhibit QS. The binding mode of the test compounds on the Cvi receptor was explored with docking studies and molecular dynamics. It was found that 8-pentyloxyphenyl-2-imidazoline **13** reduced the production of violacein (IC50=56.38 μM) without affecting bacterial growth, suggesting inhibition of *quorum sensing*. Indeed, compound **13** is apparently one of the best QS inhibitors known to date. Molecular docking revealed the affinity of compound **13** for the orthosteric site of the *N*-hexanoyl homoserine lactone (C_6-AHL) on the CviR protein. Ten aminoacid residues in the active site of C_6-AHL interacted with **13**, and 7 of these are the same as those interacting with AHL. Contrarily, 8-octyloxyphenyl-2-imidazoline **14,** 8-decyloxyphenyl-2-imidazoline **15** and 9-decyloxyphenyl-2-oxazoline **18** bound only to an allosteric site and thus did not compete with C_6-AHL for the orthosteric site.

Keywords: Azolines synthesis, *quorum sensing*, *Chromobacterium violaceum* CV026, molecular docking, molecular dynamics.

1. Introduction

Quorum sensing (QS) is a mechanism of bacterial communication involved in regulating the expression of genes linked to the production of virulence factors, among other functions. Such virulence factors include lytic enzymes, proteases, siderophores and adhesins [1-3].

This mechanism is based on the detection of small signaling molecules called autoinducers or semiochemicals, which are synthesized and released when bacteria reach a certain population density [4].

Interrupting QS is an attractive strategy in the fight against bacteria, especially against pharmacoresistant bacteria, because the QS break does not directly affect the survival of these microorganisms [5]. Given the increasingly common antibiotic resistance displayed by bacteria, particularly in the case of hospital infections, there is an intense search for novel antibacterial agents. Hence, the development of *quorum sensing* inhibitors (QSIs), also known as *antiquorum sensing* (antiQS) molecules, could possibly be an important element in the development of new antimicrobial agents.

Compounds that function as QSIs can be obtained from plants (2,3) [6], bacteria [7], marine algae (4,5) [8], fungi (6) [9] and synthetic procedures (7,8) [10, 11]. In gram-negative bacteria, the QS system is regulated by acyl-homoserine lactones (AHLs). Bacterial enzymes of some gram-positive bacteria like the Bacillus species interfere with QS via an AHL-lactonase [12]. Various analogs and bioisosteres of AHLs have been synthesized as inhibitors of gram-negative bacteria [13], some of them designed to interfere with QS in *Chromobacterium violaceum* [14].

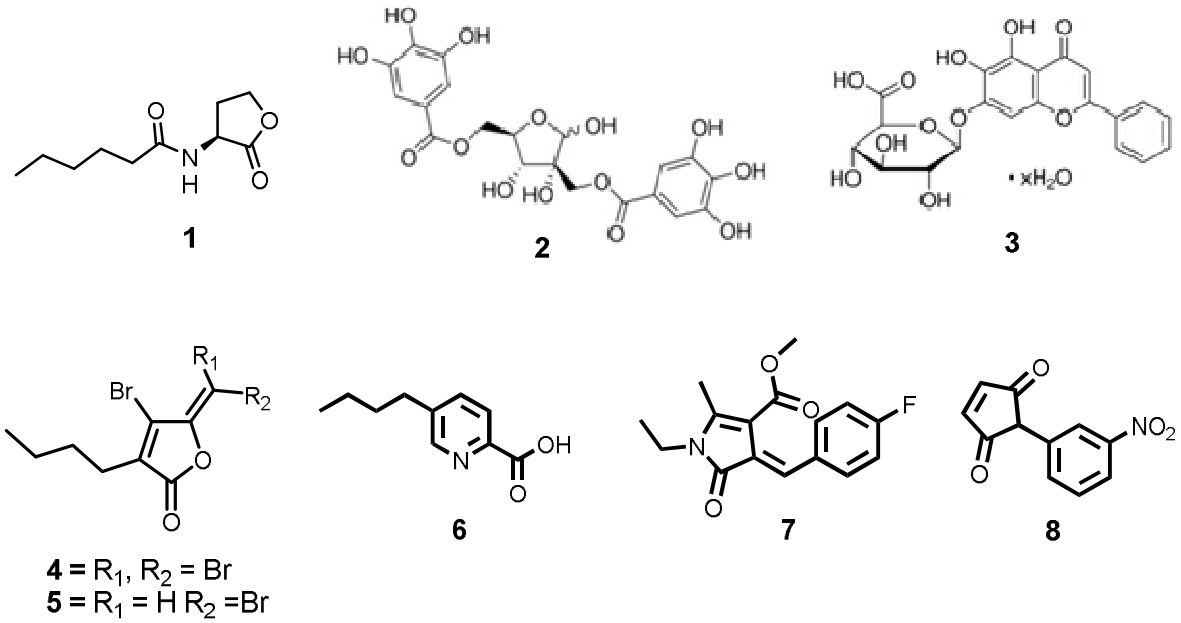

Figure 1. C_6-AHL (**1**) and *quorum sensing* inhibitors.

Chromobacterium violaceum is a gram-negative bacterium whose autoinducer is hexanoyl homoserine lactone (C_6-AHL, **1**). *C. violaceum* was herein used as a biosensor [15].

Our group previously observed [13] the potential of imidazoline **9** as a lead compound, evidenced by its 71% inhibitory activity of QS in *C. violaceum* at 100 µM (IC50 = 90.9 µM). In the present study, we sought analogs of compound **9** with improved inhibitory activity at a lower concentration. In addition to carrying out inhibition assays of the test compounds on *C. violaceum*, docking and molecular dynamics studies were performed with the same compounds to gain insights into the interactions responsible for the desired activity.

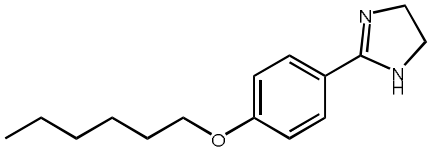

9

2. Results and Discussion

2.1. Chemistry

Six azolines were synthesized, including three 8-alkyloxyphenyl-2-imidazolines and three 9-alkyloxyphenyl-2-oxazolines, with moderate and good yields, respectively (Table 1).

Table 1. Synthesis of azolines.

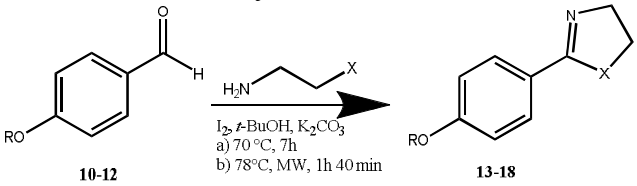

R	X	Reaction conditions	Compound number	Isolated yield (%)
n-C_5H_{11}	NH	a)	**13**	80
n-C_8H_{17}	NH	a)	**14**	79
n-$C_{10}H_{21}$	NH	a)	**15**	69
n-C_5H_{11}	O	b)	**16**	89
n-C_8H_{17}	O	b)	**17**	80
n-$C_{10}H_{21}$	O	b)	**18**	68

*C*ompound **13** has been synthesized mediated by pentyloxybenzene, 4-aminobutanoic acid, phosporic acid and P_2O_5, yield 48 % [16]. It was here synthesized with a better yield Table 1. Compound **14** has already been synthesized by 4-octyloxybenzonitrile and ethylenediamine, yield 50 % [17]. Here it was obtained with a yield of 79 %. Compound **15** was reported by Gossens *et al*. [18] as a precursor of an ionic liquid but melting point, yield and spectroscopic data are missing. They obtained compound **15** mediated by ethylenediamine and NBS. Compounds **16-18** are new. Compounds **13-1*8*** have never been employed as a QSI.

All compounds were characterized by spectroscopic methods (IR, NMR and HRMS), identifying 8-pentyloxyphenyl-2-imidazoline **13**, 8-octyloxyphenyl-2-imidazoline **14**, 8-decyloxyphenyl-2-imidazoline **15**, 9-pentyloxyphenyl-2-oxazoline **16**, 9-octyloxyphenyl-2-oxazoline **17** and 9-decyloxyphenyl-2-oxazoline **18**.

2.2. Biological activity

2.2.1. Evaluation of azolines **13-18** as *quorum sensing* inhibitors in *Chromobacterium violaceum* CV026

After synthesizing the azolines **13-18**, all were examined as possible QSIs in *C. violaceum* CV026. Since this gram-negative bacterial strain does not synthesize its own C_6-AHL, the production of violacein depends on the concentration of exogenous C_6-AHL added to the medium.

Compounds **13-18** were evaluated as QSIs at 0 (blank), 0.0001, 0.001, 0.01, 0.1, 1, 10, 100 and 1000 µM (Graph 1). Two readings were taken on a spectrophotometer to determine optical density, one at 720 nm for the culture and the other at 577 nm for the extract of violacein. These readings were used to calculate the relative violacein production, dividing the absorbance value at 577 nm by that found at 720 nm. For calculating the percentage of relative violacein production after the application of each test compound, the average of the values of the blanks was taken as 100%. The resulting percentage of violacein production was plotted as a function of the concentration of the compound. Our group previously reported [13] that a concentration of 500 nM C_6-AHL makes it easier to detect the production of violacein and its inhibition by a compound.

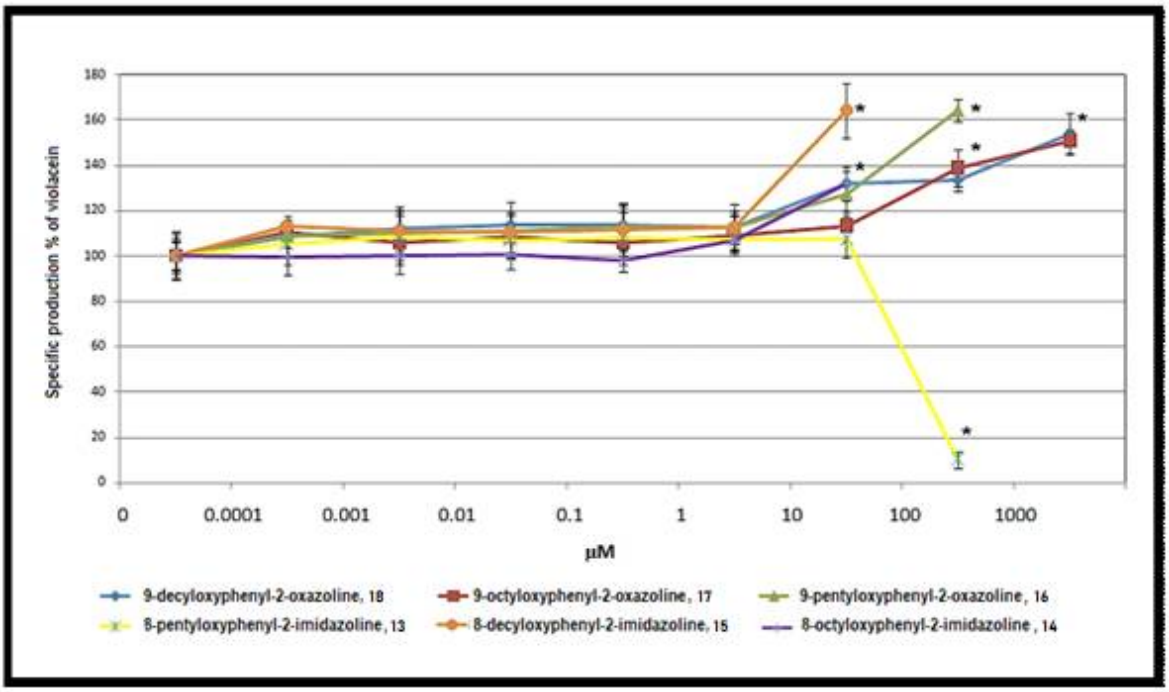

Graph 1. Production of violacein upon exposure to azolines **13-18**.

In the range of 0.0001 to 1 µm, compounds **13-18** did not cause a decrease in the percentage of violacein production. However, when the bacterium was exposed to a concentration ≥10 µm of compounds **14**, **15**, **16** and **18**, there was a significantly higher percentage of violacein production compared to the control (Graph 1). In contrast, compounds **13** and **17** at the same concentration did not stimulate such an increase in production. In fact, violacein production significantly declined with **13** at 100 µM and 1000 µM, due to a toxic effect on bacteria at these concentrations.

Although three oxazolines elevated the production of violacein at 100 µM, only two of them, oxazolines **17** and **18**, did so at 1000 µM. The latter two compounds did not have any effect on the growth of *C. violaceum* CV026. On the other hand, imidazoline **15** at concentration of 100 and 1000 µM did not trigger violacein production, but instead had an

inhibitory effect on the growth of bacteria, which was verified by the viable count. The same effect was observed with 1000 µM of oxazoline **16**. Since the 10 and 100 µM concentrations of imidazoline **13** prompted an abrupt decrease in violacein production, an experiment was conducted with concentrations of 0-100 µM (Graph 2).

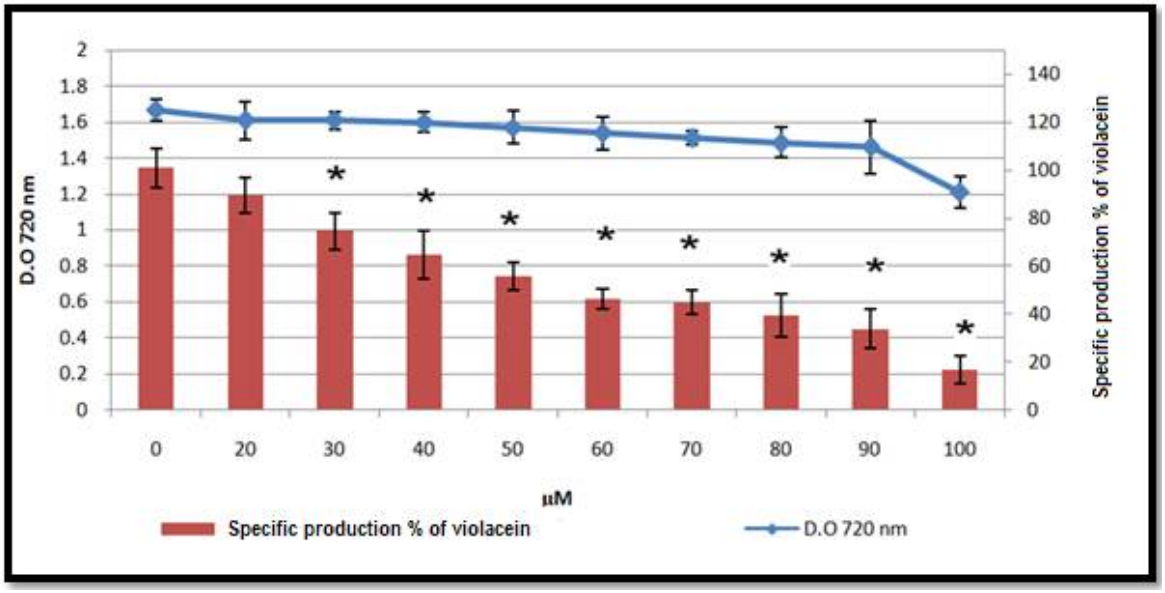

Graph 2. Optical density at 720 nm, illustrating the percentage of relative violacein production (mean ± SE; n=6) in *Chromobacterium violaceum* CV026 when exposed to different concentrations (0-100 µM) of **13**. Asterisks indicate statistically significant activity ($p < 0.05$, calculated with ANOVA).

Imidazoline **13** showed a dose-dependent behavior (Graph 2). According to the experimental data, the IC50 was calculated to be 56.38 µM. This value can be compared to those reported by Bucio *et al.* for **9, 19-23** [13, 14], **24** and the other synthesized inhibitors [19] (Figure 2).

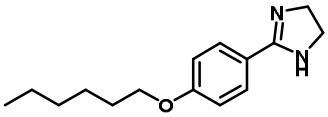

9

IC50 = 90.9 µM

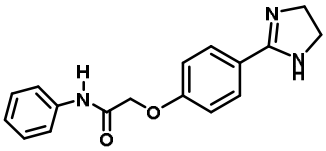

19

IC50= 66.08 µM

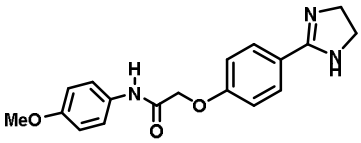

20

IC50= 340.73 µM

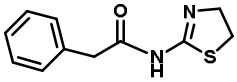

21

IC_{50}= 670.27 µM

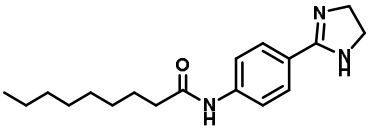

22

Active from 1 nM

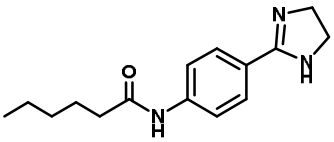

23

Active 0.1 µM

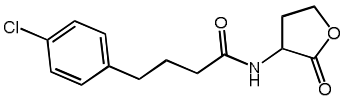

24

Figure 2. IC_{50} of some azolines evaluated as QSIs in *Chromobacterium violaceum* CV026. ND = not determined [13, 14].

Imidazoline **13** (IC50=56.38 µM) is more active than **9** (90.9 µM) [13], **19** (66.08 µM), **20** (340.73 µM) and **21** (670.27 µM) [14], and is comparable to 2-(4'-chlorophenoxy)-N-butanoyl homoserine lactone **24** [19]. The latter is proposed as the most active analog of AHL known so far, giving a total inhibition of violacein at 10^{-4} M.

Bucio et al. [13] did not give the IC50 value for *N*-[4-phenyl-(imidazo-2-yl)]-hexylamide, **23**, or *N*-[4-phenyl-(imidazo-2-yl)]-nonamide, **22**. However, they were described as active from 0.1 µM to 1 nM, respectively, on C. *violaceum* CV026. Imidazoline **13** was herein found to be active as of 30 µM. Since it was essential to examine the possibility that **13** works as an antagonist of C_6-AHL in *C. violaceum* CV026, a docking study was carried out for this ligand on the CviR protein.

2.2.2. Evaluation of imidazolines and oxazolines as agonists of C_6-AHL in *Chromobacterium violaceum* CV026

It was also crucial to determine whether the oxazolines **16-18** work as agonists of C_6-AHL in *C. violaceum*. Therefore, *C. violaceum* CV026 was incubated in the presence of each of the compounds at concentrations of 0.0001, 0.001, 0.01, 0.1, 1.10, 100 and 1000 µM, at 29 °C and 700 rpm for 24 h, without exogenous C_6-AHL. A positive control with C_6-AHL and a negative control without C_6-AHL were included. No violacein production was observed in any of the tubes containing the compounds.

Other cases of overproduction of violacein have been documented [13, 15, 20]. In 2004, Martinelli *et al*. [20] investigated several compounds in relation to their capacity to affect bacteria growth and/or activate QS in *C. violaceum* CV026 to improve the production of violacein. The most outstanding of their findings for the purposes of the current contribution is that some compounds are capable of stimulating violacein production, but only in the presence of C_6-AHL. They proposed that these compounds may either bind synergistically with C_6-AHL at the protein receptor site or interact with a second autoinductor system like the one detected in *V. harveyi*. On the other hand, Kothari and coworkers [15] suggested that enhanced violacein production is due to an overexpression of the genes participating in glucose metabolism, which after some steps would affect tryptophan biosynthesis and finally violacein biosynthesis. According to the current results, the compounds capable of elevating violacein production only did so in the presence of C_6-AHL, clearly showing that the test compounds did not perform the same function as AHL.

3. Docking simulations

Exploration was made by means of molecular coupling as to whether each compound can decrease or increase violacein production by binding to the target site on the protein. Docking was carried out with the AutoDock 4.2 Program [21]. The prior validation of docking studies involved the natural ligand C_6-AHL and the CviR protein, yielding a free energy value (ΔG) of -7.11 kcal/mol. The C_6-AHL protein made four hydrogen bond interactions with amino acid residues of the CviR active site region: (1) the carbonyl of the lactone ring with Tyr80, (2) the alpha oxygen of the lactone ring with Trp84, (3) the hydrogen of the amide with Asp97 and (4) the oxygen of the amide with Ser155. The respective distances of these four bonds were 2.56, 2.95, 2.94 and 3.28 Å, Figure 3.

The present data from the docking study of C_6-AHL on CviR coincides with the results obtained by Bucio et al. [14], who found a ΔG of -7.26 kcal/mol and the following amino acid residues in the binding region: Tyr80, Trp84, Tyr88, Asp97, Ile99, Trp111, Phe115 and Ser155, Figure 4.

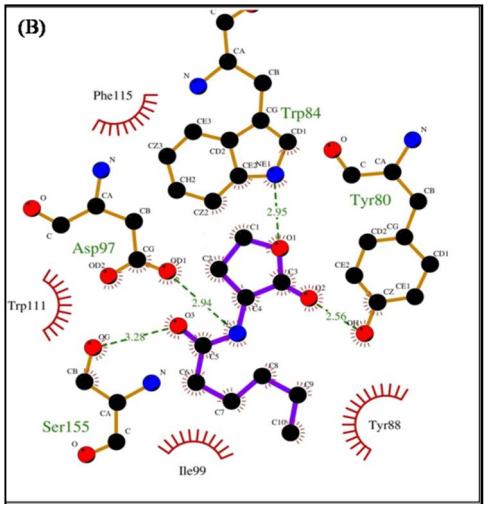

Figure 3. Schematic 2D diagram showing the interactions between *N*-hexanoyl homoserine lactone and CviR. The hydrophobic residues of the protein receptor that make contact with the ligand are represented by semicircles and radiant lines.

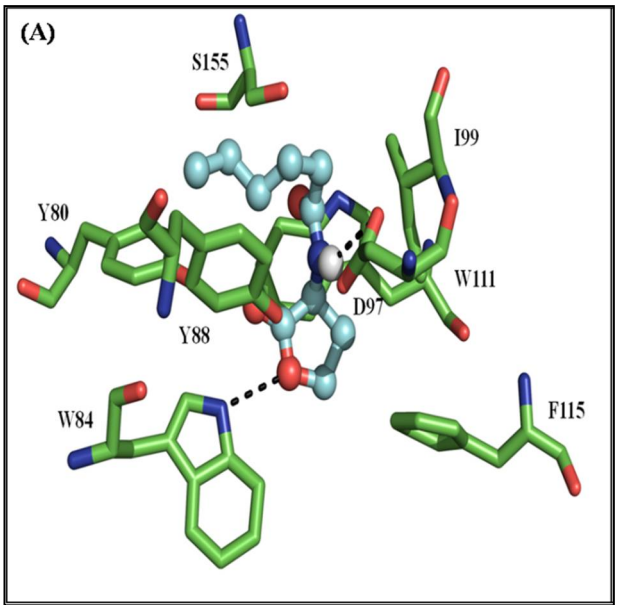

Figure 4. The interaction of N-hexanoyl homoserine lactone with CviR portrayed in 3D.

Once the docking method was validated by a simulation using a natural ligand, theoretical calculations were made for the other ligands, finding the ΔG values for the interactions and identifying the amino acid residues of CviR involved in protein-ligand binding with each compound, Table 2.

Table 2. The ΔG values for the ligand-protein interactions and the amino acid residues of the protein involved in binding.

Ligand	ΔG kcal/mol	Amino acid residues of the interaction site
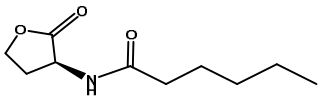 C_6-AHL, **1**	**-7.11**	Tyr80, Trp84▲,Tyr88, Asp97▲, Ile99, Trp111, Phe115, Ser155
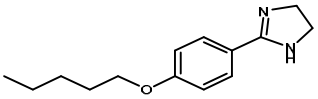 **13**	**-7.56**	Tyr80, Trp84, Tyr88, Asp97▲, Ile99, Trp111■, Phe126, Met135,Ile153, Ser155▲
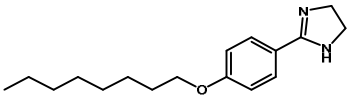 **14**	**-5.95**	Ile28, Ala31, Gly32, His177, GlnQ180, Val183, Arg184, Pro189▲
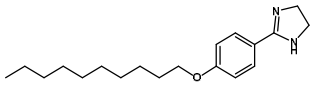 **15**	**-6.02**	Ile28,Ala31, Gly32, His177, Gln180, Val183, Arg184, Pro189▲
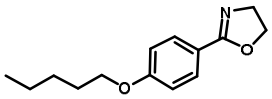 **16**	**-7.62**	Ile57, Tyr80, Trp84▲, Leu85, Tyr88, Asp97, Ile99, Trp111, Phe115, Met135 ,Ile153, Ser155▲
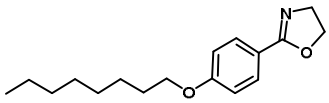 **17**	**-7.28**	Ile57, Val59, Met72, Val75, Tyr80, Trp84, Leu85, Tyr88, Ile99, Met100, Trp111, Met135, Ile153, Ser155
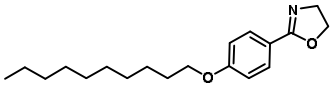 **18**	**-6.14**	Ala31, Gly32 ,His177, His179, Gln180, Ala181, Val183, Arg184, Leu188, Pro190

Hydrogen bonds (▲); π-π interactions (■).

The map of residues coordinating the binding of the test ligands, Table 2, suggests that there are two binding sites for the CviR protein. One is the orthosteric site of C_6-AHL, the

binding location of 8-pentyloxyphenyl-2-imidazoline, 9-pentyloxyphenyl-2-oxazoline and 9-octyloxyphenyl-2-oxazoline. The amino acid residues most frequently involved in interactions with these compounds are Tyr80, Trp84, Tyr88, Asp97, Ile99, Trp111, Phe115, Phe126, Met135, Ile153 and Ser155. The other binding site for the CviR protein is allosteric, the binding location of **16, 17** and **20**, most frequently involving the following residues: Ile28, Ala31, Gly32, His177, His179, Gln180, Ala181, Val183, Arg184, Leu188 and Pro190. Based on the aforementioned data, a 3D image was constructed to illustrate the overlap of the ligands in their respective binding sites, Figure 5.

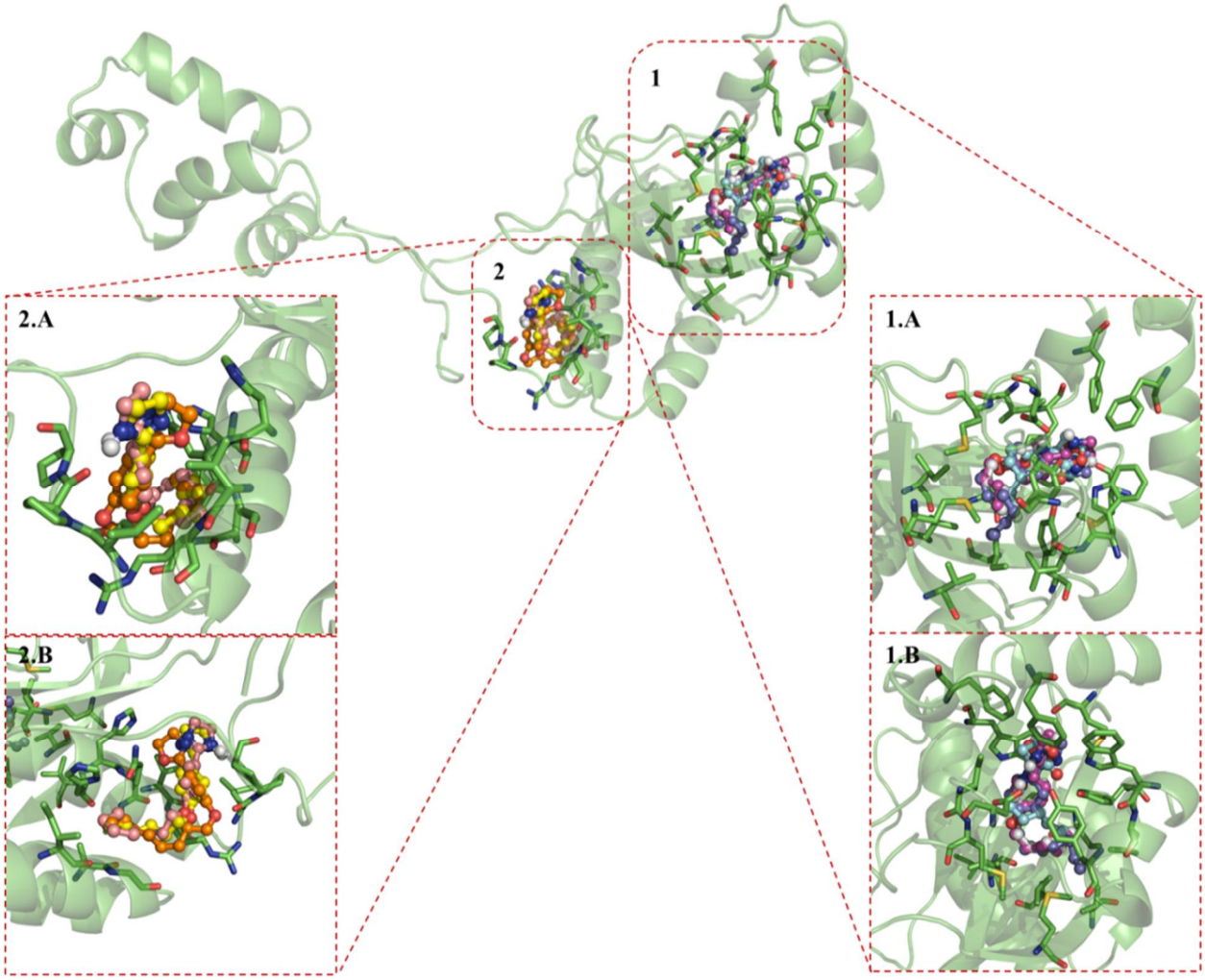

Figure 5. 3D illustration of the interaction of the ligands at two binding sites of the CviR protein, consisting of the orthosteric site and an allosteric site of C_6-AHL. (1A) Approach of the overlap of C_6-AHL, **13**, **16** and **17** with the amino acid residues of the active site of C_6-AHL. (1B) The same approach with a 45° rotation. (2A) Approach of the overlap of **14**, **15** and **18** with the amino acid residues of the allosteric site. (2B) The same approach with a 45° rotation.

The non-covalent interactions of each ligand at the orthosteric site of the CviR protein are presently described. Two hydrogen bonds are formed by the interaction of 8-pentyloxyphenyl-2-imidazoline, **13** with the CviR protein, one between the oxygen of the ether and the Ser155 residue at a distance of 2.76 Å, and the other between the hydrogen of the imidazoline ring and Asp97 at a distance of 3.16 Å. There are also hydrophobic

interactions (Van der Waals), which occur with the amino acid residues Val59, Met72, Tyr80, Trp84, Leu85, Tyr88, Ile99, Met100, Trp111, Phe115, Ph126, Met135 and I153, Figure 6. Additionally, π-π interactions are observed between the phenyl ring and W111, Figure 7.

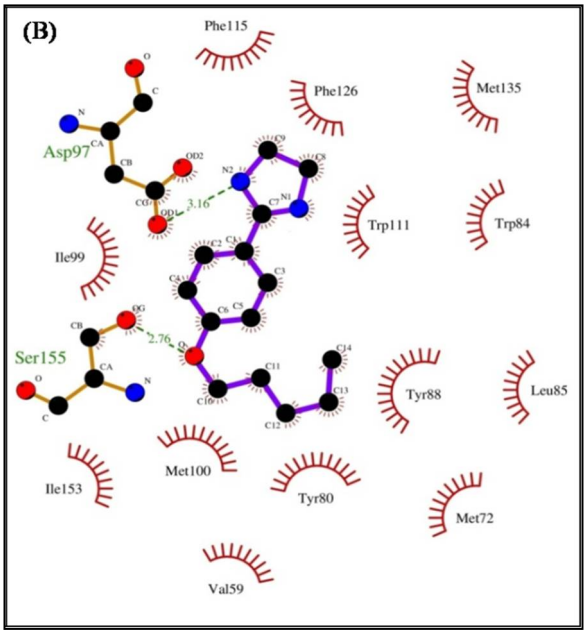

Figure 6. The non-covalent interaction of **13** with CviR. The ligand-protein interaction is illustrated **(A)** in 3D, and **(B)** in a 2D schematic diagram. Hydrogen bonds are depicted with a dotted green line, indicating the bond distance in Å (3.28). The hydrophobic residues of the protein in contact with the ligand are portrayed by red semicircles and radiant lines: Phe115 .

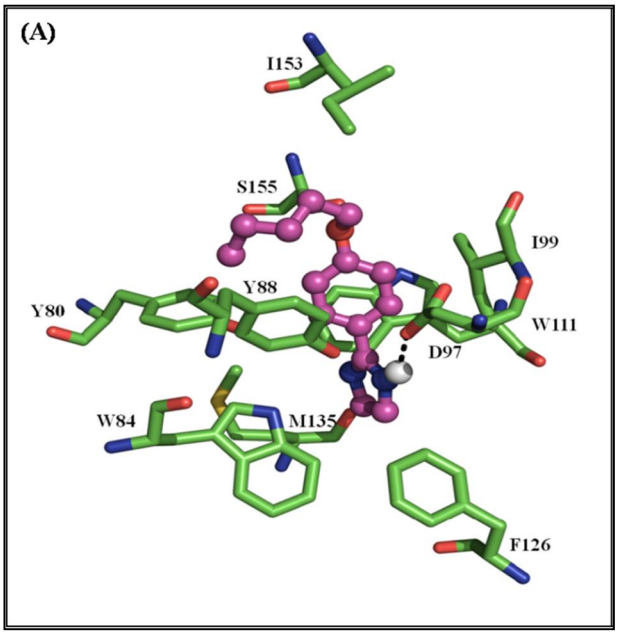

Figure 7. 3D portrayal of the π-π interactions between the phenyl ring of **13** and W111.

Compound **16** forms two hydrogen bonds, one between the oxygen of the ether and Ser155, and the other between the N of the oxazoline ring and the hydrogen of Trp84. There are also hydrophobic interactions with amino acids Ile57, Tyr80, Leu85, Tyr88, Asp97, Ile99, Trp111, Phe115, Met135 and Ile153, Figure 8.

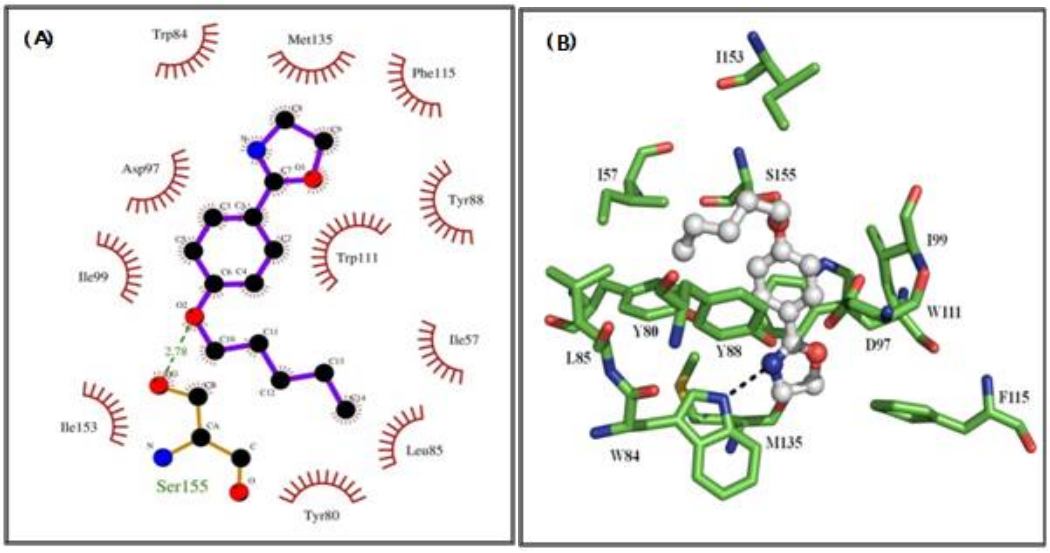

Figure 8. The interactions between oxazoline **16** and CviR (A) in a 2D schematic diagram and (B) in 3D.

Oxazoline **17** exhibits only hydrophobic interactions with amino acids Ile57, Val59, Met72, Val75, Tyr80, Trp84, Leu85, Tyr88, Ile99, Met100, Trp111, Met135, Ile153 and Ser155, Figure 9.

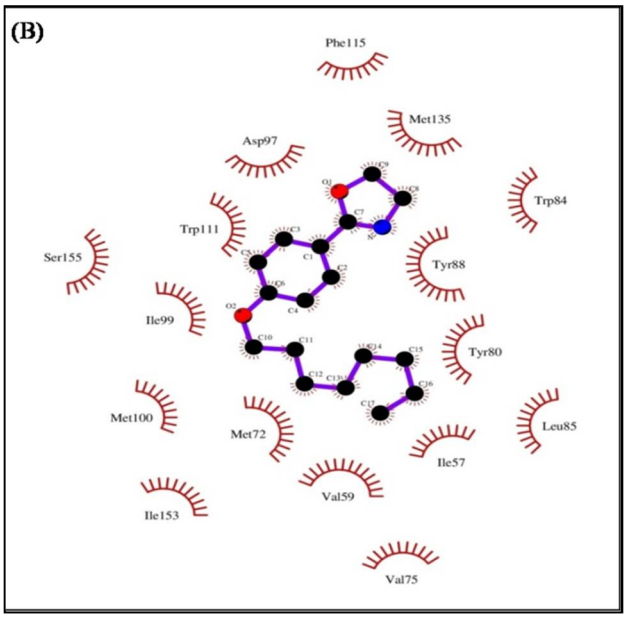

Figure 9. A 2D schematic diagram of the interaction between **17** and CviR.

Regarding the interactions between the ligands and the allosteric site, imidazoline **14** displays hydrophobic interactions with the amino acids Ile28, Ala31, Gly32, His177,

Gln180, Ala181, Val183, Arg184, Leu188 and Pro190. A hydrogen bond exists between the hydrogen of the imidazoline ring and Pro189, at a distance of 3.08 Å, Figure 10.

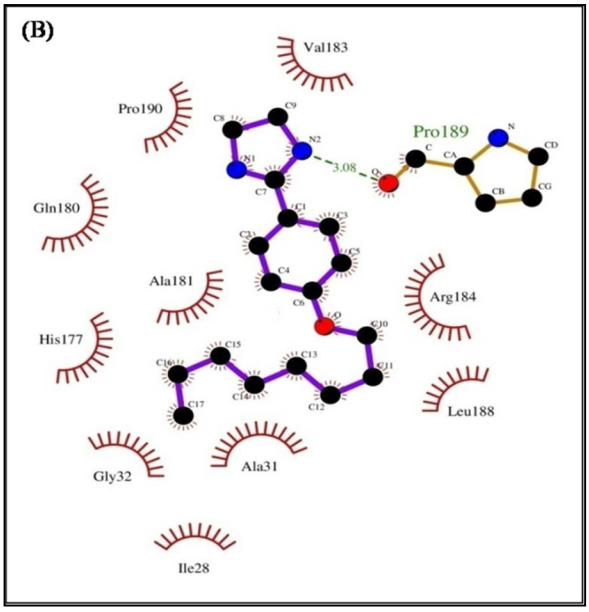

Figure 10. A 2D schematic diagram of the interaction between **14** and CviR.

Ligand **15** makes a hydrogen bond between the N-H of imidazoline and Pro189, at a distance of 2.87 Å. In addition, there are hydrophobic interactions with the amino acid residues Ile28, Ala31, Gly32, His177, Gln180, Ala181, Val183, Arg184, Leu188 and Pro190, the same interactions that were found for imidazoline **14,** Figure 11.

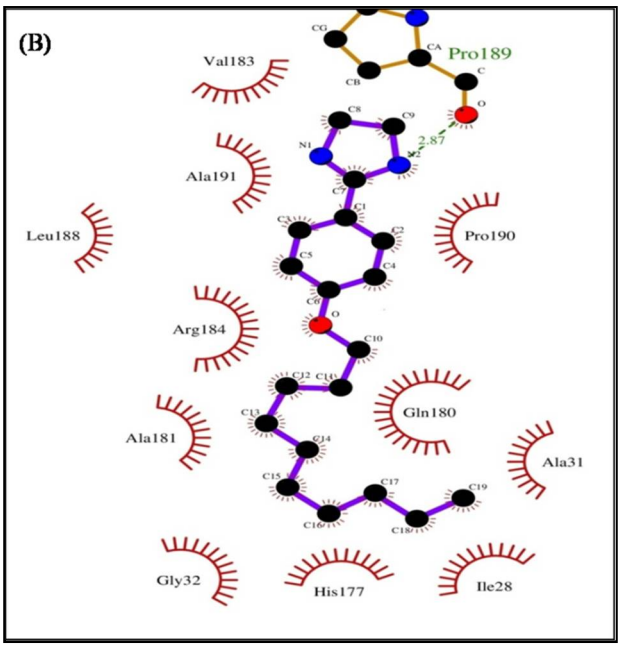

Figure 11. A 2D schematic diagram depicting the interactions between **15** and CviR.

Finally, compound **18** does not establish hydrogen bonds, but has many hydrophobic interactions with Ala31, Gly32, His177, His179, Gln180, Ala181, Val183, Arg184, Leu188 Pro 189, Ile28 and Pro190, Figures 12 and 13.

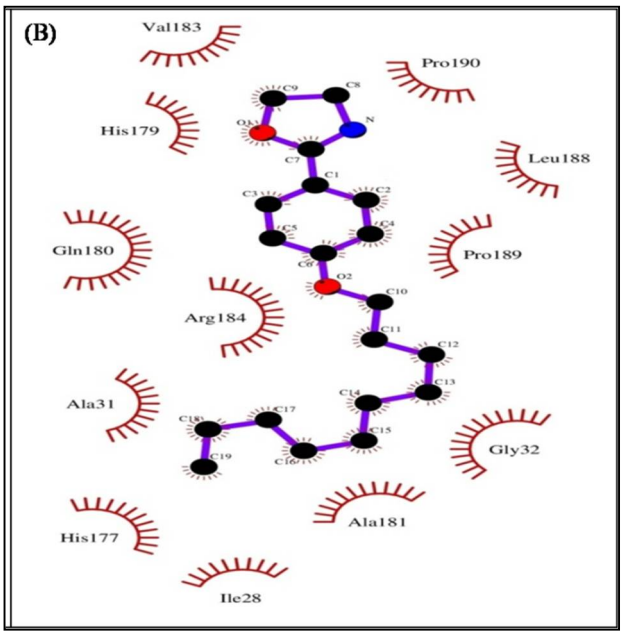

Figure 12. A 2D schematic diagram of the interaction of **18** with CviR.

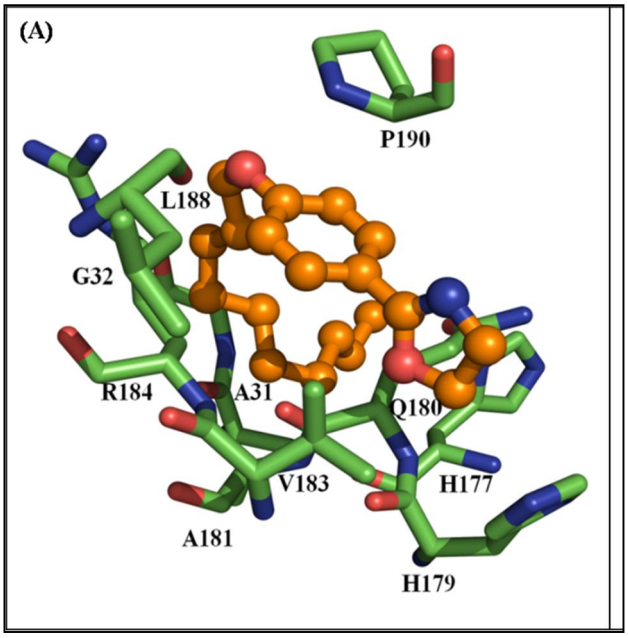

Figure 13. The interaction of **18** with CviR shown in 3D.

Molecular coupling assays indicate that imidazoline **13** can attach to the orthostatic site of C_6-AHL, opening the possibility of an antagonistic effect. This compound proved to decrease violacein production experimentally, which is in agreement with the findings reported by Bucio for hexyloxy phenylimidazoline [13].

Since ligands **14**, **15** and **18** only interact with the amino acid residues of the allosteric site, they do not compete with C_6-AHL for the orthostatic site. Such an allosteric binding mode may be due to the number of carbons in the aliphatic chain of each compound.

One hypothesis is that these compounds function as positive allosteric modulators. By binding to the allosteric site, they might trigger a modification in the orthostatic site that allows for better binding by C_6-AHL. Consequently, the protein-C_6-AHL complex would form and bind to the promoter site (vioBox), thus activating and causing an enhanced transcription of the genes encoding for the enzymes involved in the synthesis of violacein.

Regarding oxazoline **16** and oxazoline **17**, the docking studies show that they bind to the orthosteric site of C_6-AHL. Although these compounds elicited a high production of violacein experimentally, they were unable to produce violacein in the absence of C_6-AHL. Hence, they are not agonists.

4. Molecular dynamics, binding free energy calculations and per-residue decomposition

During docking simulations, all atoms of the receptor remained fixed. It was necessary to incorporate flexibility and solvation for all atoms of the protein-ligand complex during the docking calculations of the predicted complexes to achieve a more reliable result. Therefore, molecular dynamics simulations were conducted to examine the preservation of the CviR-ligand complexes for compounds **13**, **14** and **16**.

To assess the stability of the complexes, first a RMSD analysis was made to determine the appropriate time period for a structural and energetic evaluation once reaching the equilibration stages. The CviR-**13**, CviR-**14** and CviR-**16** systems reached equilibrated RMSD fluctuations during the first 10 ns, with average values ranging from 5.65 to 8.7 Å. Accordingly, the first 10 ns were excluded from the 50-ns-long MD simulations for the subsequent clustering analysis and binding free energy calculations.

The relative binding free energy (ΔG_{mmgbsa}), established with the MM/GBSA approach for examining CviR-ligand interactions show that all these complexes are thermodynamically favorable for binding. The main energetic contribution to ΔG_{mmgbsa} was guided by the nonpolar contributions ($\Delta E_{non\text{-}polar}$), while the polar contributions (ΔE_{polar}) were found to be unfavorable for the protein-ligand association (Table 3). The comparison of the different protein-ligand systems of the test compounds revealed that **13** and **16**, which both target the orthosteric site, bind with similar affinity. Interestingly, they exhibit a less favorable ΔG_{mmgbsa} value than **14**, even though the latter targets the allosteric site.

Table 3. Binding free energy components of protein-ligand complexes (in units of kcal/mol).

System	ΔE_{vdw}	ΔE_{ele}	$\Delta G_{ele,sol}$	$\Delta G_{npol,sol}$	$\Delta E_{non\text{-}polar}$	ΔE_{polar}	DG_{mmgbsa}
13	-37.86 (0.22)	-6.07 (0.21)	21.38 (0.18)	-5.35 (0.02)	-43.21	15.31	-27.90 (0.23)
15	-45.77 (0.27)	-11.32 (0.30)	24.02 (0.26)	-5.96 (0.02)	-51.73	12.7	-39.03 (0.35)
16	-33.95	-14.21	24.69	-5.08	-39.03	10.48	-28.55

	(0.30)	(0.26)	(0.20)	(0.03)			(0.27)

The polar ($\Delta E_{polar} = \Delta E_{ele} + \Delta G_{ele,sol}$) and non-polar ($\Delta E_{non\text{-}polar} = \Delta E_{vwd} + \Delta G_{npol,sol}$) contributions. Energy is expressed in kcal/mol (± standard error of the mean) and averaged over 400 snapshots at time intervals of 100 ps taken during 40 ns (after ignoring the first 10 ns of MD simulations).

To dissect the contribution of each residue to binding, analysis was made of the per-residue decomposition of each of the residues contributing to ΔG_{mmgbsa}. The key residues involved in binding and the per-residue free energy ($\Delta E_{per\text{-}residue}$) were examined for the CviR-**13,** Figure 14 A-B, CviR-**16,** Figure 14 C-D and CviR-**14,** Figure 14 E-F complexes, Figure 14. It turns out that the CviR-**13,** Figure 14 A-B and CviR-**16,** Figure 14 C-D, complexes are stabilized by many of the same residues. Nonetheless, the chemical differences between them leads distinct residues to provide greater contributions to the ΔG_{mmgbsa} value: Ile57, Ile99, Met100 and Trp111 for CviR-**13,** Figure 14 A-B and Ile57, Met72, Tyr88 and Met100 for CviR-**16,** Figure 14 C-D. Ile57 and Met100 are present in the stabilization of both **13** and **16**, suggesting a crucial role for these residues in molecular recognition at the orthosteric site. For **14,** Figure 14 E-F, on the other hand, the non-polar protein environment implicated in stabilization is lesser for the allosteric than orthosteric site. Pro6, Gln180, Arg184 and Pro190 contribute most to the ΔG_{mmgbsa} value. They may be crucial residues for stabilization at the allosteric site.

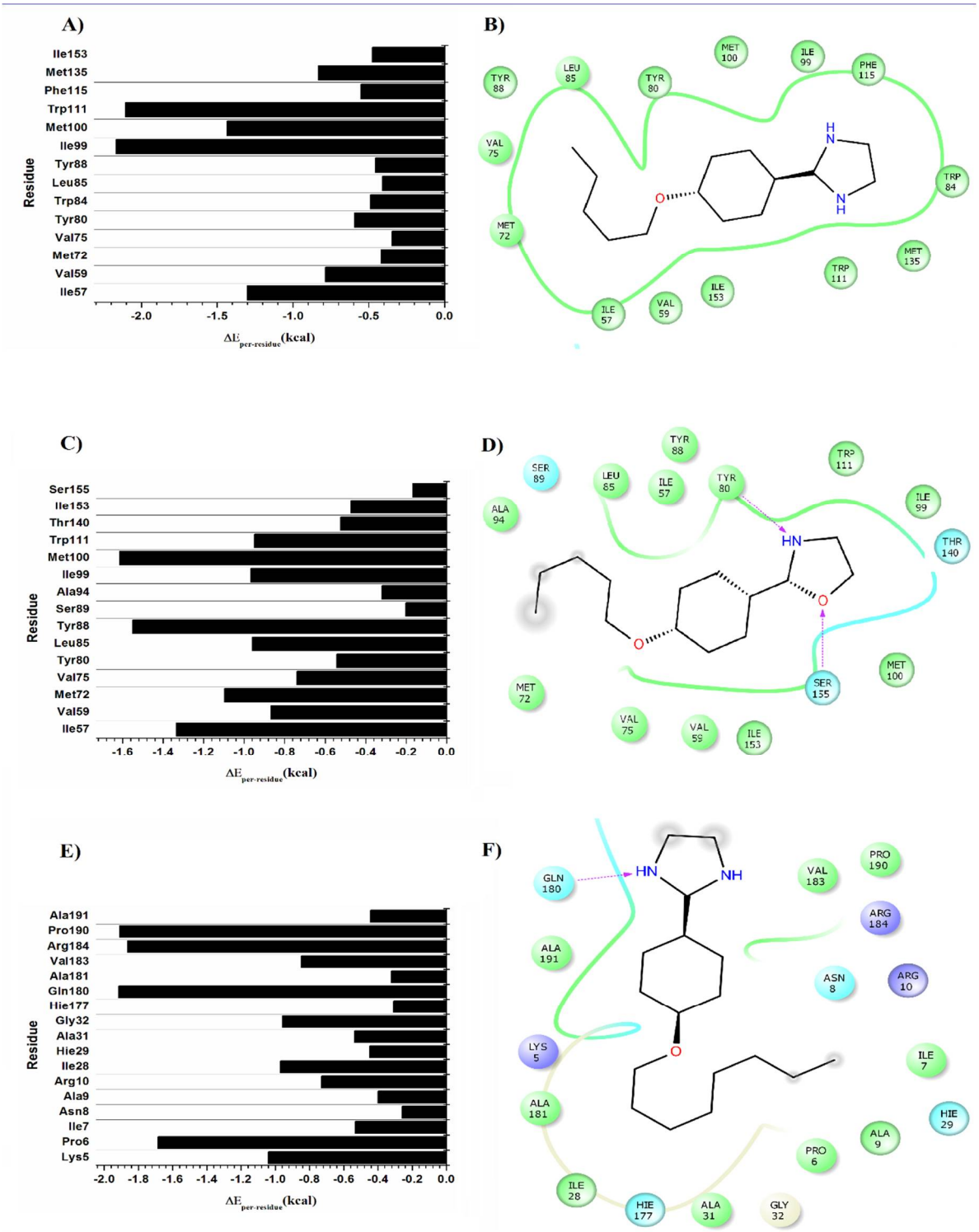

Figure 14. Per-residue free energy ($\Delta E_{per\text{-}residue}$) and map of interactions for the most populated conformation of the CviR-**13** (A and B), CviR-**16** (C and D) and CviR-**14** (E and F) complexes. The map of interactions was constructed with Maestro Schrödinger version 10.5 [22].

5. Materials and Methods

5.1. Drying and purification of solvents

Ethyl acetate, methylene chloride and hexane were purified by fractional distillation with calcium oxide (CaO) as the drying agent. The solvents were refluxed for 5 h before carrying out distillation. Ethylenediamine was also purified by fractional distillation, in this case with metallic sodium, and refluxed under nitrogen atmosphere for 1 h. Ethylenediamine was stored at 5 °C under nitrogen atmosphere and protected from light.

5.2. Characterization of the synthesized compounds

The organic compounds were characterized by NMR spectroscopy, mass spectrometry (MS) and infrared (IR) spectroscopy. ^{1}H and ^{13}C NMR spectra NMR were recorded on a Varian Mercury spectrometer at 300 and 75 MHz and on a Varian 500 Mercury spectrometer at 500 and 125 MHz, respectively. Infrared (IR) spectra were obtained on a Perkin Elmer FT-IR spectrum 2000 spectrometer from the ENCB-IPN spectroscopy instrumentation center. HRMS was performed with a JEOL-JSM-GC mate II and LRMS ESI(+) and spectra were recorded using a BRUKER MicrOTOF QII. Melting points were determined on an electrothermal apparatus and are uncorrected.

5.3. Synthesis of alkylated aldehydes [13]

In a 25 mL two-neck flask, adapted with a refrigerant and magnetic stirrer and kept under nitrogen atmosphere (N_2), 4-hydroxybenzaldehyde (4.09 X 10^{-3} mmol) and potassium carbonate (K_2CO_3) (8.19 X 10^{-3} mmol, 2 eq.) were added with a funnel for solids. Subsequently, 10 mL of distilled acetone were injected into the flask and the mixture was heated to reflux with constant stirring for 90 min. Then the corresponding alkyl halide (5.05 X 10^{-3} moles, 1.5 eq.) was added and the reaction mixture was maintained at reflux with constant stirring while being monitored by TLC. After the reaction ended, the mixture was cooled to room temperature (rt), filtered and extracted with methylene chloride (CH_2Cl_2), and the solvent was evaporated under reduced pressure in a rotary evaporator. The product was purified by silica gel column chromatography by using a polarity gradient of hexane-ethyl acetate. The fractions containing pure product were evaporated under reduced pressure and finally dried under a high vacuum. The resulting substances were characterized by NMR, IR and HRMS.

***para*-pentyloxy benzaldehyde (10)**

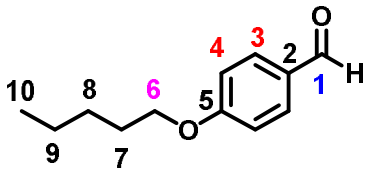

Oil at rt

IR (KBr)

ν= 3074 (C-H), 2931, 2870 (C-H), 1688 (C=O), 1262, 1027 (=C-O-C), 830.

^{1}H NMR ($CDCl_3$)

δ= 9.82 (s, 1H, CHO), 7.35 (AA'BB', 4H, Ar), 3.98 (t, 2H, OCH_2), 1.76 (q, 2H, H-7), 1.38 (m, 4H, H-8 y H-9), 0.90 (t, 3H, CH_3).

^{13}C NMR ($CDCl_3$)

δ= 190.47 (CHO), 164.06 (C-5), 131.73 (C-3), 129.56 (C-2), 114.54 (C-4), 68.19 (C-6), 28.55 (C-7), 27.91 (C-8), 22.21 (C-9), 13.78 (C-10).

***para*-octyloxy benzaldehyde (11)**

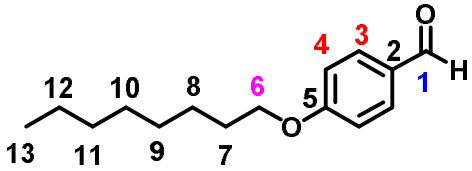

Oil at rt

IR (KBr)

ν= 3074 (C-H), 2925, 2855 (C-H), 1693 (C=O), 1255, 1019 (=C-O-C), 830.

^{1}H NMR ($CDCl_3$)

δ= 9.71 (s, 1H, CHO), 7.24 (AA'BB', 4H, Ar), 3.86 (t, 2H, OCH_2), 1.65 (q, 2H, H-7), 1.31 (m, 2H, H-8), 1.18 (m, 8H, H-9 al H-12), 0.76 (t, 3H, CH_3).

^{13}C NMR ($CDCl_3$)

δ= 189.91 (CHO), 163.77 (C-5), 131.39 (C-3), 129.40 (C-2), 114.27 (C-4), 67.92 (C-6), 31.39 (C-7), 28.92 (C-8), 28.82 (C-9), 28.66 (C-10), 25.56 (C-11), 22.24 (C-12), 13.65 (C-13).

***para*-decyloxy benzaldehyde (12)**

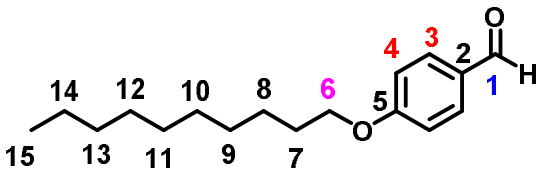

Oil at rt

IR (KBr)

ν= 3074 (C-H), 2923, 2854 (C-H), 1696 (C=O), 1258, 1016 (=C-O-C), 831.

^{1}H NMR ($CDCl_3$)

δ= 9.81 (s, 1H, CHO), 7.33 (AA'BB', 4H, Ar), 3.96 (t, 2H, OCH_2), 1.75 (q, 2H, H-7), 1.41 (m, 2H, H-8), 1.27 (m, 12H, H-9 al H-14), 0.84 (t, 3H, CH_3).

^{13}C NMR ($CDCl_3$)

δ= 190.37 (CHO), 164.06 (C-5), 131.70 (C-3), 129.58 (C-2), 114.53 (C-4), 68.20 (C-6), 31.71 (C-7), 29.38 (C-8), 29.17 (C-9), 29.14 (C-10), 28.88 (C-11), 25.78 (C-12), 22.49 (C-13), 13.95 (C-14), 13.87 (C-15).

5.4. Synthesis of imidazolines

In a two-neck 25 mL balloon flask adapted with a refrigerant and magnetic stirrer and kept under nitrogen atmosphere and at rt, 1 eq. of the corresponding aldehyde was added followed by the injection of 8 mL of tert-butanol and 1.1 eq. of ethylenediamine. Ninety min later, 3 eq. of K_2CO_3 and 1.25 eq. of molecular I_2 were added and the temperature was raised to 70 °C. The reaction of the mixture lasted 5 h and was monitored by TLC. The system was allowed to reach rt before adding water to the reaction flask and carrying out extractions with ethyl acetate. The organic phase was washed with a saturated solution of sodium sulfite and then with a 20% NaCl solution, and subsequently dried with anhydrous sodium sulfate. The organic phases were combined and the solvent was evaporated. The remaining residue was recrystallized from ethyl acetate.

8-pentyloxyphenyl-2-imidazoline (13)

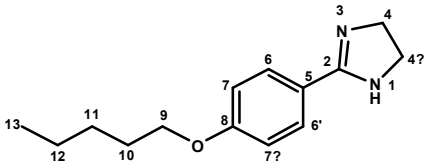

m.p. 105-107 ºC from AcOEt. 55°C from petroleum ether; b.p.125°/0.01Torr. [16]. IR (KBr), υ= 3203 cm^{-1} (NH), 1618 (C=N). ^{1}H NMR (DMSO-D_6) δ = 7.34 (AA ´BB´, 4H, Ph), 3.98 (t, 2H, H-9), 3.56 (s, 4H, H-4, H-4´), 1.71 (qi, 2H, H-10), 1.36 (m, 4H, H-11, H-12), 0.89 (t, 3H, CH_3). ^{13}C NMR (DMSO-D_6) δ= 163.03 (C-2), 160.00 (C-8), 128.45 (C-6), 122.78 (C-5), 113.70 (C-7), 67.34 (C-9), 49.17 (C-4, C-4´), 28.14 (C-10), 27.51 (C-11), 21.17 (C-12), 13.71 (C-13). HRMS, m/z = calculated for $C_{14}H_{21}N_2O$ (M^+): 233.1648; found 233.1625.

8-octyloxyphenyl-2-imidazoline (14)

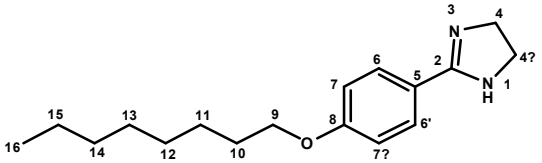

m.p. 115-117 ºC from AcOEt. m.p.109 °C from benzene:hexane [17].IR (KBr) υ = 3209 cm^{-1} (NH), 1618 (C=N). ^{1}H NMR (DMSO-D_6)δ = 6.95 (AA ´BB´,4H, Ph), 3.99 (t, 2H, H-9), 3.60 (s, 4H, H-4, H-4´), 1.72 (qi, 2H, H-10), 1.39 (m, 2H, H-11), 1.27 (m, 8H, H-12, H-13, H-14, H-15), 0.86 (t, 3H, CH_3). ^{13}C NMR (DMSO-D_6) δ =163.28 (C-2), 160.43 (C-8), 128.77 (C-6), 122.23 (C-5),113.96 (C-7), 67.57 (C-9), 49.10 (C-4,C-4´), 31.12 (C-10), 28.72 (C-11), 28.65 (C-12), 28.60 (C-13), 25.48 (C-14), 22.07 (C-15),13.93 (C-16). HRMS, m/z = calculated for $C_{17}H_{26}N_2O$ (M^+): 275.2118; found 275.2099.

8-decyloxyphenyl-2-imidazoline (15)

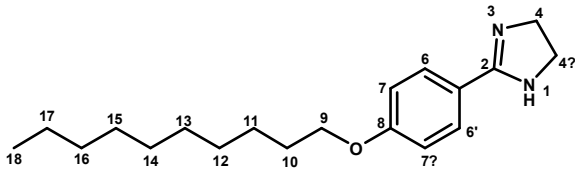

m.p. 151-153 ºC IR (KBr), υ = 3132cm^{-1} (NH), 1614 (C=N). ^{1}H NMR (DMSO-D$_6$) δ = 7.56 (AA ´BB´,4H, Ph), 4.09 (t, 2H, H-9), 3.98 (s, 4H, H-4, H-4´), 1.73 (qi, 2H, H-10), 1.41 (m, 2H, H-11), 1.29 (m, 12H, H-12, H-13, H-14, H-15, H-16, H-17), 0.84 (t, 3H, CH$_3$). ^{13}C NMR (DMSO-D$_6$) δ = 164.43 (C-2), 163.67 (C-8), 130.79 (C-6), 115.32 (C-7), 113.93 (C-5), 68.38 (C-9), 44.35 (C-4,C-4´), 31.42 (C-10), 29.12 (C-11), 29.07.18 (C-12), 28.84 (C-13), 28.82 (C-14), 28.56 (C-15), 25.53 (C-16), 22.23 (C-17),14.08 (C-18). HRMS, m/z = calculated for $C_{19}H_{30}N_2O$ (M^+): 303.2431; found 303.2467.

5.5. Synthesis of oxazolines

To a 200 mL MW reactor flask, adapted with a refrigerant and a magnetic stirrer, was added 1 eq. of the corresponding aldehyde (depending on the oxazoline to be synthesized) followed by the injection of 5 mL of t-BuOH and 1.1 eq. of ethanolamine. The flask was placed in a chemical microwave oven (model MIC-1, Prendo) and the conditions for the reaction were programmed (50 °C, 3 min 14 s, 1290 rpm and 60% power at 762 watts). After this cycle, addition was made of 3 eq. of K_2CO_3 and then of 1.5 eq. of I_2 and the reaction conditions were changed (78 °C, 20 min 14 s, 1290 rpm and 60% power at 762 Watts). The reaction, monitored by TLC, ended upon completion of 5 cycles. Once the system reached rt, the organic phase was separated and water was added to the reaction flask. Potassium carbonate was solubilized (aqueous phase) and extractions were carried out by using ethyl acetate. The organic phase was washed with a saturated solution of sodium sulfite (Na_2SO_3) and then with a 20% NaCl solution, and subsequently dried with anhydrous sodium sulfate. The ethyl acetate was evaporated under reduced pressure. The mixture of the product and remaining raw material were separated by silica gel column chromatography by using a polarity gradient of hexane-ethyl acetate. The solvent was evaporated from the pure fractions and the purified product dried under a high vacuum.

9-pentyloxy phenyl-2-oxazoline (16)

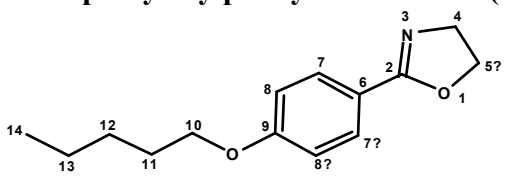

m.p. 36-38 ºC. IR (KBr), υ = 1649 cm^{-1} (C=N). ^{1}H NMR (DMSO-D$_6$) δ = 6.96 (AA ´BB´,4H, Ph), 4.35 (t, 2H, H-5), 3.99 (t, 2H H-10), 3.90 (t, 2H, H-4), 1.71 (m, H-11), 1.35 (m, H-12, H-13), 0.88 (t, 3H, CH$_3$). ^{13}C NMR (DMSO-D$_6$) δ =162.70 (C-2), 161.06 (C-9), 129.46 (C-7), 119.81 (C-6), 114.35 (C-8), 67.68 (C-10), 67.18 (C-5), 54.37 (C-4), 28.31 (C-11), 27.67 (C-12), 21.91 (C-13), 13.97 (C-14). HRMS, m/z = calculated for $C_{14}H_{29}NO_2$ (M^+): 234.1489; found 234.1529.

9-octyloxy phenyl-2-oxazoline (17)

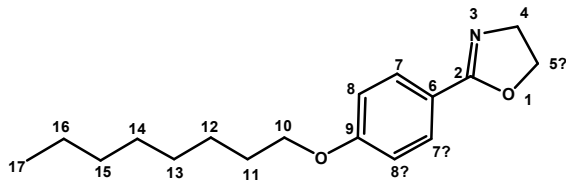

m.p. 41-43ºC. IR (KBr), υ = 1644 cm^{-1} (C=N). ^{1}H NMR (CDCl$_3$) δ = 6.88 (AA ´BB´,4H, Ph), 4.39 (t, 2H, H-5), 4.03 (t, 2H, H-10) ,3.98 (t, 2H, H-4), 1.78 (m, 2H, H-11),

1.45 (m, 2H, H-12), 1.32 (m, 8H, H-13, H-14, H-15, H-16) 0.88 (t, 3H, CH_3). ^{13}C NMR ($CDCl_3$) δ = 165.16 (C-2), 161.69 (C-9), 127.01 (C-7),117.05 (C-6), 111.37 (C-8), 65.33 (C-10), 64.68 (C-5), 52.08 (C-4), 29.04 (C-11), 26.55 (C-12), 26.43 (C-13), 26.38 (C-14), 23.23 (C-15), 19.88 (C-16), 11.31 (C-17). HRMS, m/z = calculated for $C_{17}H_{25}NO_2$ (M^+): 276.1958; found 276.2000.

9-decyloxy phenyl-2-oxazoline (18)

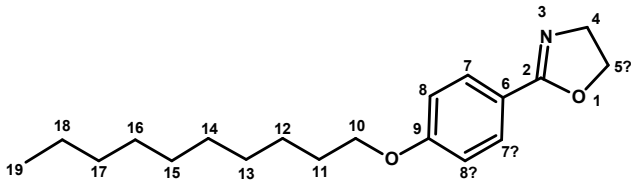

m.p. 48-50ºC.IR (KBr), υ =1650 cm^{-1} (C=N). ^1H NMR (DMSO-D_6) δ = 6.97(AA´BB´,4H, Ph), 4.35 (t, 2H, H-5), 4.00 (t, 2H, H-10), 3.91 (t, 4H, H-4, H-4´), 1.71 (m, 2H, H-11), 1.40 (m, 2H, H-12), 1.28 (m, 12H, H-13, H-14, H-15, H-16, H-17, H18), 0.85 (t, 3H,CH_3). ^{13}C NMR (DMSO-D_6) δ = 162.65 (C-2), 161.00 (C-9), 129.41 (C-7),119.75 (C-6),114.31 (C-8), 67.63 (C-10), 67.13 (C-5), 54.31 (C-4), 31.28 (C-11), 28.98 (C-12), 28.93 (C-13), 28.73 (C-14), 28.68 (C-15), 28.55 (C-16), 25.44 (C-17), 22.08 (C-18), 13.92 (C-19). HRMS, m/z = calculated for $C_{19}H_{29}N0_2$ (M^+):304.246; found 304.2316.

5.6. Preparation of culture media, test compounds and inoculum

The Luria Bertani (LB) broth was prepared in one liter of distilled water by adding 10 g peptone, 5 g yeast extract and 5 g NaCl, then sterilized in an autoclave at 15 psi and 121 °C for 15 min. For the LB solid medium, 15 g of bacteriological agar was added to a liter of distilled water. *C. violaceum* CV026 was always grown in the presence of 30 µg/mL of kanamycin.

The amount of each compound required for a concentration of 100 mM was weighed. With the resulting solution, serial dilutions 1:10 were made to obtain the concentrations of 10 mM, 1 mM, 100 µM, 10 µM, 1 µM, 100 nM and 10 nM.

From the cryovials containing *C. violaceum* CV026, a roast was taken and crosswise streaked in a box containing LB agar and 30 µg/mL kanamycin, followed by incubation at 29 °C for 24 h. A roast was also taken from an isolated colony and inoculated in 5 mL LB medium with 30 µg/mL kanamycin for CV026, followed by incubation at 29 °C and 200 rpm for 15 h. Finally, the boxes were stored in refrigeration.

5.7. Evaluation of the compounds as quorum sensing inhibitors in **Chromobacterium violaceum** *CV026*

C. violaceum CV026 was cultured in 60 mL of LB medium with 30 µg/mL kanamycin until reaching an optical density of 0.1 to 600 nm. Subsequently, in 2 mL tubes were placed 980 µL of this culture, 80 µM C_6-AHL (800 nM final concentration), and 10 µL of the dilutions of the test compounds until reaching the final concentration of 1 mM, 100 µM, 10 µM, 1 µM, 100 nM, 10 nM, 1 nM or 100 pM. Then the tubes were incubated at 29 °C and 700 rpm for 24 h. Upon completion of the incubation time, cell density was determined by absorbance at 720 nm by using LB medium as the blank. Finally, the absorbance of violacein was measured.

5.8. Evaluation of violacein

500 µL of the bacterial culture were placed in a 2 mL tube and 500 µL of acetone were added. The tubes were vortexed and centrifuged at 15000 rpm for 4 min to prepare for the determination of the absorbance of violacein in the supernatants at 577 nm. The specific production of violacein was calculated by dividing the value of the reading at 577 nm by that at 720 nm. Each experiment was performed 6 times/compound and the results were graphed. Statistical significance was analyzed by ANOVA.

5.9. Viable count

From the 24-h cultures of the test compounds, 10 µL were taken to make decimal dilutions and 5 µL of each dilution was dripped onto plates containing LB agar. After incubation at 29 °C for 24 h, the colonies on each spot were counted. These assays were performed in triplicate, and viable counts were confirmed by standard bacterial plating.

5.10. Assay of the compounds as agonists

A flask containing 60 mL of LB medium with kanamycin was adjusted to an optical density of 0.1 to 600 nm with *C. violaceum* CV026. Subsequently, 990 µL of this solution were placed in 2 mL tubes and 10 µL of the dilutions of the compounds were added until reaching a final concentration of 1mM, 100µM, 10µM, 1µM, 100 nM, 10 nM, 1nM or 100 pM. Moreover, a positive control (990µL culture + 10 µL of an 80 µM solution of C_6-AHL) and a negative control (990µL culture + 10µL of LB medium) were included. The tubes were incubated at 29 °C while subjected to shaking at 700 rpm for 24 h. The presence or absence of pigment was then observed to make an evaluation of violacein.

5.11. Determination of MIC in Chromobacterium violaceum CV026

The procedure described in section 5.7 was followed, except that the final concentration of the compounds was from 10 to 1000 µM. The MIC was assigned to the lowest concentration of the compound yielding no bacterial development.

5.12. Modeling and optimization of ligands

Docking studies were carried out on the ligands tested experimentally in *C. violaceum* CB026 and on the natural ligand of the CviR protein. The ligands were built with the ACD/ChemSketch program, creating a geometric pre-optimization in 3D (respecting the stereochemistry and spatial configuration). The structures were saved in .mol format, and these files served as input to create the Z matrix for each molecule on the GaussView 5.0 graphical visualizer. The files were saved in .gjp input format for use in Gaussian 09. The structures obtained (and their respective matrices Z) were submitted to a geometric and energetic optimization at the AM1 semi-empirical level with the chemical-quantum package of Gaussian 09. The output files in .out format were transformed into 3D format .pdb with the GaussView 5.0 program. The latter files were utilized for simulations by molecular coupling.

5.13. Molecular studies

With docking studies, an initial examination was made of each ligand binding site on the CviR protein as well as the ligand-receptor interactions. *C. violaceum* 12472 (located in the Protein Data Bank under the PDB code: 3QP6) was chosen as the target protein for this analysis on the AutoDock 4.2 program, which maintains the macromolecule rigid while

allowing flexibility in the ligand [23]. The AutoDock 4.2 program has shown good correlation between the free energy values of the binding simulations and the experimental data [24]. Blind docking was carried out with a grid box of 126 x 126 x 126 Å and a 0.375 Å space between grid points,[3] and by using the Hybrid Genetic Algorithm of Lamarckian with an initial population of 100 randomized individuals and a maximum number of energy evaluations of $1x10^7$. The results of the simulations were examined by means of the PyMol visualizer, observing the amino acid residues of the protein involved in the interactions with the ligands. 2D protein-ligand interaction diagrams were generated with the LIGPLOT program, revealing additional amino acid residues that interact with the ligands.

5.14. Molecular dynamics simulations and binding free energy calculations

MD simulations of the CviR-ligand systems were conducted with the PMEMD module AMBER 12 package [25], the ff99SB force field [26] and the generalized Amber forcefield (GAFF) [27]. A 12 Å rectangular-shaped box of TIP3P water molecules [28] was constructed to solvate the CviR-ligand complexes, and counterions were placed at different locations to neutralize the charges of the complexes at pH 7. Systems were minimized and equilibrated by carrying out a protocol that began with 1000 steps of steepest descent minimization and continued with 1000 steps of conjugate gradient minimization. Equilibrations began by heating the systems from 0 to 310 K during 200 picoseconds (ps) of MD simulations, with position restraints set at a constant volume. Successive MD simulations were conducted under periodic boundary conditions (PBCs) using an isothermal isobaric (NpT) ensemble of 200 ps to adjust the solvent density, followed by 800 ps of constant pressure equilibration at 310K (with the SHAKE algorithm) [29] on hydrogen atoms using a time step of 2 femtoseconds (fs) and Langevin dynamics for temperature control. Subsequent to equilibrations, 50 ns-long MD simulations were conducted in the absence of position restraints, under PBCs and with an NpT ensemble at 310K. A 10 Å cut-off was applied for the van der Waals interactions. The electrostatic term was described via the particle mesh Ewald method [30] and bond lengths were constrained at their equilibrium values with the SHAKE algorithm [29]. Temperature and pressure were maintained by utilizing the weak-coupling algorithm [31] with coupling constants τ_T and τ_P of 1.0 and 0.2 ps, respectively (310 K, 1 atm). The time-dependence of the MD simulation runs was analyzed by employing AmberTools from Amber12. On the other hand, structural representations were created with PyMOL v0.99 [32] and Maestro Schrödinger version 10.5 [22].

5.15. Calculation of absolute binding free energies and per-residue contributions

Absolute binding free energies were calculated according to the MMGBSA [33] (Miller., 2012; [34] Kollman et al., 2000; [35]Gohlke et al., 2004; [36]Onufriev et al., 2004) provided in Amber12 [25](Case et al., 2005). For this purpose, 400 snapshots at time intervals of 100 ps were extracted during 40 ns, ignoring the first 10 ns of the 50-ns-long MD simulations, using a salt concentration of 0.1 M and the Born implicit solvent model [35] (Onufriev et al., 2004) after removing water molecules and counterions. The analyses were performed with the MMPBSA Perl script [34](Gohlke et al., 2004). The binding free energy of each complex can be calculated as follows:

$$\Delta G_{mmgbsa} = G^{complex} - G^{receptor} - G^{ligand}$$

$$\Delta G_{bind} = \Delta E_{MM} + \Delta G_{solvation} - T\Delta S$$

6. Conclusions

Six azolines were synthesized, including three imidazolines obtained in moderate yields by conventional heating and three oxazolines afforded in good yields by MW. The performance of the azolines was dependent on the size of the chains of the alkoxy benzaldehydes. A significant increase in violacein production was induced (in the presence of hexanoyl homoserine lactone) by 8-decyloxyphenyl-2-imidazoline **17** (**15**) (10 μM), 9-decyloxyphenyl-2-oxazoline **20** (**18**) (10, 100 and 1000 μM), 9-pentyloxyphenyl-2-oxazoline **18** (**16**) (10 and 100 μM) and 9-octyloxyphenyl-2-oxazoline **19** (**17**) (100 and 1000 μM). An inhibitory effect on violacein production was shown by 8-pentyloxyphenyl-2-imidazoline **15** (**13**), with an IC_{50} of 56.38 μM, strongly suggesting an *antiquorum sensing* effect. This was the most active compound in the homologous series. Of the imidazolines currently under study, those with anti-QS activity had an aliphatic chain similar in size to that of C_6-AHL. An inhibitory effect on the growth of *C. violaceum* CV026 was elicited by 100 and 1000 μM of imidazoline **17** (**15**), 100 μM of imidazoline **16** (**14**) and 1000 μM of oxazoline **18** (**16**). *Quorum sensing* agonist activity was not found for any of the test compounds. The experimental inhibitory effect on violacein production promoted by **15** (**13**) was in agreement with the docking study. Ten amino acid residues in the active site of the receptor protein were involved in the interactions with 8-pentyloxyphenyl-2-imidazoline. Seven of these 10 also interacted with AHL. Additionally, one of them is implicated in π-π interactions.

Author Contributions: *Conceptualization, A.R.-A.; methodology, A.R.-A.,E.C.-Q. and J.C.-B.; software, J.C.-B., M.B. and J.L.H.-A; validation, A.R.-A.,E.C.-Q. and J.C.-B.; formal analysis, A.R.-A., E.C.-Q., J.C.-B., J.L.H-A. and M.B.; investigation, J.L.H-A., M.B.; resources, A.R.-A.,E.C.-Q. and J.C.-B.; data curation, A.R.-A.; writing—original draft preparation, A.R.-A., E.C.-Q. and J.C.-B; writing—review and editing, A.R.-A.; visualization, A.R.-A.; supervision, A.R.-A., E.C.-Q. and J.C.-B.; project administration, A.R.-A.; funding acquisition, A.R.-A.*

Funding: *"This research was funded by CONACYT, grant number 240808" and by IPN grant number SIP20181765".*

Supplementary Material: Selected ^{1}H NMR-, ^{13}C NMR-. HSQC- HMBC- IR-, HRMS-Spectra

Acknowledgments: AR is grateful to the IPN for financial support through grants SIP20181765 and to Conacyt for grant 240808. JLHA is appreciative of scholarships provided by Conacyt and the IPN. We are beholden to CNMN, IPN, for HRMS and to CE, ENCB, for IR spectra.

Conflicts of Interest: The authors declare that they have no conflict of interest.

References

1. Dunny, G.M.; Leonard, B.A. Cell-cell communication in gram-positive bacteria. Annu. Rev. Microbiol. **1997**, 51, 527–564. doi.org/10.1146/annurev.micro.51.1.527.
2. Miller, M.B.; Bassler, B.L. *Quorum sensing* in bacteria. Annu. Rev. Microbiol. **2001**, 55, 165–199. DOI: 10.1146/annurev.micro.55.1.165.
3. Jayaraman, A.; Wood, T.K. Bacterial *quorum sensing*: signals, circuits, and implications for biofilms and disease. Annu Rev Biomed Eng. **2008** 10: 145–167. doi: 10.1146/annurev.bioeng.10.061807.160536.

4. Fuqua, C; Greenberg, E.P. Listening in on bacteria: acyl-homoserine lactone signalling. Nat. Rev. Mol. Cell Biol. **2002**, 3, 685–695. DOI:10.1038/nrm907
5. Joseph P. Gerdt and Helen E. Blackwell. Competition Studies Confirm Two Major Barriers That Can Preclude the Spread of Resistance to Quorum-Sensing Inhibitors in Bacteria. | ACS Chem. Biol. 2014, 9, 2291−2299. dx.doi.org/10.1021/cb5004288.
6. Chong-Lek, K.; Choon-Kook, S.; Wai-Fong, Y.; Li,Ying, T.; Thiba, K.; Yee, M., Ch.; Kok-Gan, Ch. Plant-derived natural products as sources of anti-quorum sensing compounds. Sensors **2013**, 13 (5), 6217-6228. doi:10.3390/s130506217.
7. By de la Fuente, M.; Miranda, C.D.; Jopia, P.; Gonzalez-Rocha, G.; Guiliani, N.; Sossa, K.; Urrutia, H. Growth inhibition of bacterial fish pathogens and quorum sensing blocking by bacteria recovered from Chilean salmonid farms. J. Aquat. Anim. Health. **2015**, 27, 112-122. DOI: 10.1080/08997659.2014.1001534.
8. Manefield, M., De Nys, R., Kumar, N., Read, R., Givskov, M., Steinberg, P., Kjelleberg, S. Evidence that halogenated furanones from Delisea pulchra inhibit acylated homoserine lactone (AHL)-mediated gene expression by displacing the AHL signal from its receptor protein. Microbiology **1999**,145, 283–291. Doi: 10.1099/13500872-145-2-283.
9. Majumdar, S.; Mondal, S. Perspectives on Quorum Sensing in Fungi. IJMBM, **2015**, 6, 170-180. ISSN: 2165-0136.
10. Welsh, M. A.; Eibergen, N. R.; Moore, Joseph D.; Blackwell, H. E. Small Molecule Disruption of Quorum Sensing Cross-Regulation in Pseudomonas aeruginosa Causes Major and Unexpected Alterations to Virulence Phenotypes. J Am Chem Soc. **2015**, 137 , 1510-1519. DOI: 10.1021/ja5110798.
11. Galvan, J. E.; Defonsi Lestard, M. E.; Piro, O. E.; Echeverria, G.; Molina, R. D. I.; Arena, M. E.; Ulic, S. E.; Tuttolomondo, M. E.; Ben Altabef, A. Synthesis, characterization and crystal structure of 2-Chloroethyl(methylsulfonyl)methanesulfonate. New Journal of Chemistry. **2018**, 42, 11073-11084. ISSN:1144-0546. DOI:10.1039/C7NJ05138G

12. Maisuria, VB.; Nerurkar, AS. Interference of *Quorum Sensing* by Delftia sp. VM4 Depends on the Activity of a Novel N-Acylhomoserine Lactone-Acylase. PLOS ONE. **2015**, 10(9): e0138034. doi.org/10.1371.
13. Reyes-Arellano, A.; Bucio-Cano, A.; Montenegro-Sustaita M.; Curiel-Quesada, E.; Salgado-Zamora, H. Imidazolines as Non-Classical Bioisosteres of N-Acyl Homoserine Lactones and *Quorum Sensing* Inhibitors. Int. J. Mol. Sci. **2012**, 13, 1284-1299; doi:10.3390/ijms13021284.
14. Bucio Cano A., Reyes Arellano A., Correa Basurto J., Bello M., Torres Jaramillo J., Salgado-Zamora H., Curiel-Quesada E, Peralta-Cruz J, Avila-Sorrosa A. Targeting *quorum sensing* by designing azoline derivatives to inhibit the N-hexanoyl homoserine lactone-receptor CviR: Synthesis as well as biological and theoretical evaluations. Bioorg. Med. Chem. **2015**, 23, 7565–7577. doi.org/10.1016/j.bmc.2015.10.046
15. Kothari, V.; and Sakshi Sharma, S.; Padia, D. Recent research advances on *Chromobacterium violaceum*. Asian Pac J Trop Med. **2017**,10, 744-752. doi: 10.1016/j.apjtm.2017.07.022.
16. Walter Koller und Paul Schlac. Ein news Darstellungsverfahren für 2-Aryl-Δ^1-pyrroline und 2-Aryl-Δ^1-piperideine. Chemische Berichte **1963**, 96, 93-113. doi:10.1002/cber.19630960110
17. Harfenist, Morton; Soroko, Francis E.; McKenzie, Gerald M. 2-(Alkoxyaryl)-2-imidazoline Monoamine Oxidase Inhibitors with Antidepressant Activity. Journal of Medicinal Chemistry **1978**, 21, 4, 405-9. DOI: 10.1021/jm00202a021.
18. Goossens, K.; Wellens, S.; Van Hecke, K.; Van Meervelt, L.; Cardinaels, T.; Binnemans, K.. T-Shaped Ionic Liquid Crystals Based on the Imidazolium Motif: Exploring Substitution of the C-2 Imidazolium Carbon Atom. Chemistry - A European Journal. **2011**, 17, 15, 4291-4306. DOI:10.1002/chem.201001921.
19. Chen, G.; Swem, L.R.; Swem, D.L.; Stauff, D.L.; O'Loughlin, C.T.; Jeffrey, P.D.; Bassler, B.L.; Hughson, F.M. A strategy for antagonizing *quorum sensing*. Mol. Cell **2011**, 42, 199–209. DOI: 10.1016/j.molcel.2011.04.003.

20. Martinelli, D.; Grossmann, G.; Séquin, U.; Brandl, H.; Bachofen, R. Effects of natural and chemically synthesized furanones on *Quorum Sensing* in *Chromobacterium violaceum*. BMC Microbiol. **2004**, 4, 25. DOI: 10.1186/1471-2180-4-25.
21. Morris, G.M.; Huey, R.; W. Lindstrom, M.F. Sanner, R.K. Belew, Goodsell, S. D. Olson, A.J. AutoDock4 and AutoDockTools4: Automated docking with selective receptor flexiblity, J. Comput. Chem. **2009**, 30, 2785–2791. doi: 10.1002/jcc.21256
22. Maestro, version 10.5. Schrödinger, LLC; New York, NY, USA: **2016**–1.
23. Morris, G.M.; Goodsell, S. D.; Robert S. Halliday, R. S.; Huey, R.; Hart, E. W.; Richard, K.; Belew, K. R.; Olson, J. A. Automated docking using a Lamarckian genetic algorithm and an empirical binding free energy function. J. Comput. Chem. **1998**, 19, 14, 1639-1662. doi.org/10.1002/(SICI)1096-987X(19981115)19:14<1639::AID-JCC10>3.0.CO;2-B.
24. Patronov, A.; Ivan Dimitrov, I.; Flower, R.D.; Doytchinova, I. Peptide binding prediction for the human class II MHC allele HLA-DP2: a molecular docking approach. *BMC Structural Biology* **2011**, **11**:32. doi.org/10.1186/1472-6807-11-32.
25. Case D.A., Cheatham T.E., Darden T., Gohlke H., Luo R., Merz K.M., Onufriev A., Simmerling C., Wang B., Woods R.J.. The Amber biomolecular simulation programs. J. Comput. Chem. **2005**, 16: 1668-1688. DOI: 10.1002/jcc.20290.
26. Duan Y., Wu C., Chowdhury S., Lee M. C., Xiong Guoming, Zhang W., Yang R., Cieplak P., Luo R., Lee T., Caldwell J., Wang J., Kollman P. A point-charge force field for molecular mechanics simulations of proteins based on condensed-phase quantum mechanical calculations. J. Comput. Chem. **2003**, *24*(16), 1999-2012. DOI: 10.1002/jcc.10349
27. Wang J., Wolf R. M., Caldwell J. W., Kollman P. A., Case D. A. Development and Testing of a General Amber Force Field. J. Comput. Chem. **2004**, 25 (9). 1157-1174. DOI: 10.1002/jcc.20035
28. Jorgensen W.L., Chandrasekhar J., Madura J.D., Impey R.W., Klein M.L. Comparison of simple potential functions for simulating liquid water. J. Chem. Phys. **1983,** 79, 926-935. doi:10.1063/1.445869

29. Van Gunsteren, W. F.; Berendsen, H. J. C. Algorithms for macromolecular dynamics and constraint dynamics. Molecular Physics. Molecular Physics. **1977**, 34 (5), 1327. doi.org/10.1080/00268977700102571

30. Darden T., York D. & Pedersen L. J. Particle mesh Ewald: An N–log (N) method for Ewald sums in large systems. J. Chem. Phys. **1993**, 98 (12). 10089. DOI: doi.org/10.1063/1.464397

31. Berendsen, H.J.C. Postma, J.P.M.., van Gunsteren, W.F.; DiNola A.; Haak J. R. Molecular dynamics with coupling to an external bath. J. Chem. Phys. **1984**, 81 (8). 3684. doi.org/10.1063/1.448118.

32. DeLano WL. The PyMOL Molecular Graphics System. Palo Alto, CA, USA. http://www.pymol.org

33. Miller B.R., McGee T.D., Swails J.M., Homeyer N., Gohlke H., Roitberg A. MMPBSA.py: An Efficient Program for End-State Free Energy Calculations. Journal of Chemical Theory and Computation. **2012**, 8 (9), 3321. MMPBSA.py: an efficient program for end-state free energy calculations. J. Chem. Theory Comput. 8:3314-3321. DOI: 10.1021/ct300418h

34. Kollman P.A., Massova I., Reyes C., Kuhn B., Huo S., Chong L., Lee M., Lee T., Duan Y., Wang W., Donini O., Cieplak P., Srinivasan J., Case D.A. & Cheatham T.E. Calculating structures and free energies of complex molecules: combining molecular mechanics and continuum models. Acc. Chem. Res. **2000**, 12, 897. DOI: 10.1021/ar0001057.

35. Gohlke J.; Griffith W. & Faustman E.M. The role of cell death during neocortical neurogenesis and synaptogenesis: Implications from a computational model for the rat and mouse. Developmental Brain Research. **2004**, 151, 54. DOI: 10.1002/prot.20033

36. Onufriev, A.; Bashford, D.; Case, D.A. Exploring protein native states and largescale conformational changes with a modified generalized born model, Proteins. **2004**, 55, 383–394. DOI:10.1002/prot.20033

Sample Availability: Samples of all the compounds are available from the corresponding author.